

# Blinking Statistics Correlated with Nanoparticle Number

Siyang Wang,<sup>†</sup> Claudia Querner,<sup>†</sup> Michael D. Fischbein,<sup>†</sup> Lauren Willis,<sup>†</sup>  
Dmitry S. Novikov,<sup>‡</sup> Catherine H. Crouch,<sup>§</sup> and Marija Drndic<sup>\*,†</sup>

Department of Physics and Astronomy, University of Pennsylvania, Philadelphia, Pennsylvania 19104, Department of Physics, Yale University, New Haven, Connecticut 06520, and Department of Physics and Astronomy, Swarthmore College, Swarthmore, Pennsylvania 19081

Received September 4, 2008; Revised Manuscript Received September 22, 2008

## ABSTRACT

We report fluorescence of single semiconductor nanorods (NRs) and few-NR clusters, correlated with transmission electron microscopy for direct determination of the number of NRs present in a single fluorescent source. For samples drop-cast from dilute solutions, we show that the majority of the blinking sources (~75%) are individual NRs while the remaining sources are small clusters consisting of up to 15 NRs. Clusters containing two or three NRs exhibit intermittent fluorescence intensity trajectories,  $I(t)$ , similar to those of individual NRs. The associated statistical parameters of *on*- and *off*-time probability densities for two- and three-NR clusters are indistinguishable from those of individual NRs. In contrast, statistically distinguishable blinking parameters are observed for clusters of five or more particles. In particular, the “truncation time” of the *on*-time probability density, i.e., the time characterizing the transition from a power law to an exponential decay, was found to increase superlinearly with the number of particles. Our long ( $2.4 \times 10^4$  s) blinking measurements also directly reveal the previously unobserved truncation of the power law distribution of the *off*-times for single nanoparticles.

Many molecular and nanoscale systems have been observed to emit light intermittently, i.e., to “blink”, under continuous illumination. Examples of blinking systems include single molecules, fluorescent green protein, light harvesting complexes, organic fluorophores, and semiconductor nanoparticles.<sup>1</sup> The fluorescence intermittency displayed by many types of single emitters does not follow a simple two-level quantum jump model. In semiconductor quantum dots,<sup>1,2</sup> rods,<sup>3</sup> and wires,<sup>4</sup> in particular, the distributions of fluorescence *on*- and *off*-times of individual particles follow approximately power law (Levy) statistics.

Previous work<sup>1</sup> to explain blinking in quantum dots focused on single emitters and ensembles of independent emitters. Although a few studies used photon emission statistics<sup>5</sup> or spectral measurements<sup>6</sup> to unambiguously identify single particles, most blinking studies rely on careful sample preparation from extremely dilute nanoparticle solutions and assume that well-dispersed nanoparticles result. In such studies, some blinking sources could in fact be clusters of a few particles. Recently, fluorescence from clusters of close-packed spherical nanocrystals (NCs) was observed to fluctuate more rapidly than isolated NCs blinking indepen-

dently; the fluorescence from single emitters and clusters displayed distinguishable autocorrelation functions.<sup>7</sup> Using correlated fluorescence and atomic force microscopy, the authors determined the effective volume of the clusters, but not the number of or distance between the particles in the clusters.

We used correlated fluorescence microscopy and transmission electron microscopy (TEM) to determine the number and arrangement of CdSe nanorods (NRs) corresponding to each fluorescent source. This approach<sup>8</sup> allows for direct particle counting and high-resolution imaging. We report the fluorescence intensity versus time,  $I(t)$ , of NR clusters containing  $N = 1-15$  NRs, correlated with TEM imaging to determine the number of particles,  $N$ , the distance between NRs,  $d$ , and the angle of NRs,  $\theta$ , relative to each other and to the laser polarization direction. We find that samples drop-cast from dilute solutions with concentration  $\sim 10^{-9}$  mol·L<sup>-1</sup> are mostly comprised of individual emitters, but ~25% of blinking sources correspond to clusters of particles. Clusters consisting of two or three NRs exhibit fluorescence intermittency similar to that of individual NRs, and we show that probability density analysis does not unambiguously distinguish between individual NRs and such small clusters. Clusters of approximately five or more particles are clearly distinguishable by their longer truncation times of the *on*-time probability densities,  $\tau_c^{on}$ , and their emission intensities. The very long fluorescence measurements ( $\sim 2.4 \times 10^4$  s)

\* To whom correspondence should be addressed: e-mail, drndic@physics.upenn.edu; phone, (215) 898-5810; fax, (215) 898-2010.

<sup>†</sup> University of Pennsylvania.

<sup>‡</sup> Yale University.

<sup>§</sup> Swarthmore College.

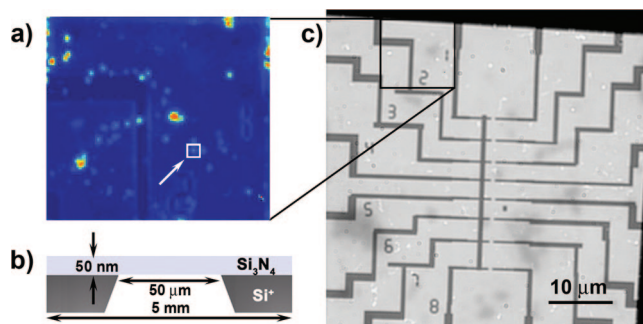


**Figure 1.** (a) Fluorescence micrograph of a  $\sim 10 \times 10 \mu\text{m}^2$  region, where a blinking movie was taken. The arrow indicates the location of the two NRs shown in Figure 4b. (b) Schematic (side view) of the  $\text{Si}_3\text{N}_4$  membrane device. (c) TEM of the transparent window region ( $\sim 50 \times 50 \mu\text{m}^2$ ) patterned with gold markers. The rectangle indicates the area of the fluorescence image. The dark border is the membrane region on top of the p-doped Si that is not TEM transparent.

also allow us to directly observe the truncation to the Levy distribution of the *off*-times.

The blinking characteristics of NRs are very similar to those of spherical nanocrystals: the distribution of *off*-times follows a power law while the distribution of *on*-times follows a truncated power law

$$P(t_{\text{on}}) \propto t_{\text{on}}^{-\alpha_{\text{on}}} e^{-t_{\text{on}}/\tau_c^{\text{on}}}$$

where  $\alpha_{\text{on}}$  is the power-law exponent and  $\tau_c^{\text{on}}$  is the truncation time.<sup>3</sup> The primary difference is that for NRs the truncation time,  $\tau_c^{\text{on}}$ , is smaller than that for spherical NCs; for NCs, typically  $\tau_c^{\text{on}} > 10$  s while for NRs,  $\tau_c^{\text{on}}$  is in the range of  $\sim 1$ – $10$  s, with larger aspect ratio NRs giving smaller  $\tau_c^{\text{on}}$ .<sup>3</sup> We attribute the smaller truncation time of the *on*-time probability density observed in larger aspect ratio NRs to a combination of larger absorption cross section, weaker quantum confinement, and possibly a higher incidence of internal trap states.<sup>3</sup> We used NRs rather than NCs for this study partly because the elongated shapes make it easier to unambiguously distinguish isolated NRs from the background features of the substrate. In addition, for NRs and NCs with the same diameter, the rod shape gives NRs a higher absorption cross section.

We used TOPO-capped CdSe/ZnSe/ZnS core/double shell semiconductor NRs, with a  $5.8 \times 34$  nm optically active CdSe core and an overall size of  $8 \times 38$  nm.<sup>9</sup> Low stress  $\sim 50$  nm thick silicon nitride ( $\text{Si}_3\text{N}_4$ ) membranes<sup>10</sup> were used as substrates because they are electron transparent in TEM and show low fluorescence background.<sup>8</sup> Gold markers, to aid in locating the NRs, were fabricated on the membrane by electron beam lithography (Figure 1).

NR solutions in toluene ( $10^{-9}$  mol·L<sup>-1</sup>) were deposited onto the substrate by drop-casting ( $1 \mu\text{L}$ ). Wide-field fluorescence imaging was performed at room temperature in air, using an epi-fluorescence microscope (Nikon Eclipse 80i) with a Nikon Apo  $100 \times 0.95$  NA dry objective and a  $670 \pm 25$  nm emission filter (Chroma 670/50M). The sample was illuminated at 488 nm ( $100 \text{ W}\cdot\text{cm}^{-2}$ ) with a continuous-wave solid-state laser (Coherent Sapphire). Fluorescence movies (10 frames/s, up to  $\sim 2.4 \times 10^4$  s long) were captured by a thermoelectrically cooled CCD camera (Princeton

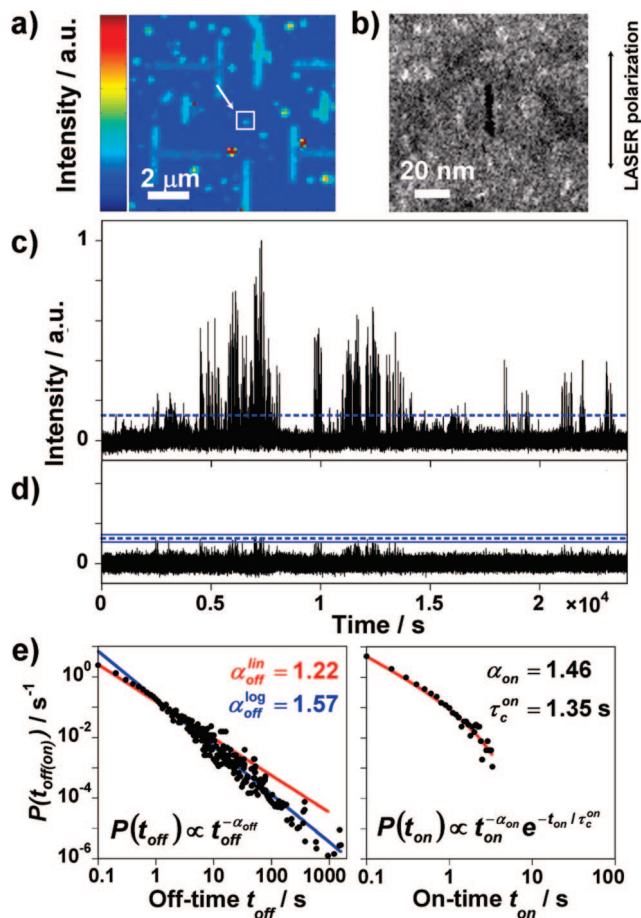


**Figure 2.** (a) Fluorescence micrograph and (b) TEM image of an individual CdSe/ZnSe/ZnS core/double shell NR, oriented approximately parallel to the laser polarization. (c) Fluorescence intensity vs time,  $I(t)$ , for this NR (dashed line indicates *on*-/*off*-threshold). (d) Fluorescence intensity vs time,  $I(t)$ , of a nearby dark region. Dashed blue line indicates the *on*-/*off*-threshold defined as  $m_{\text{dark}} + 7\sigma_{\text{dark}}$  (as used in (c)), where  $m_{\text{dark}}$  is the mean and  $\sigma_{\text{dark}}$  is the standard deviation of the corresponding intensity vs time of the dark region. The two solid blue lines correspond to  $m_{\text{dark}} + 6\sigma_{\text{dark}}$  and  $m_{\text{dark}} + 8\sigma_{\text{dark}}$ , respectively (see also Supporting Information). (e) Probability densities of *off*-times (left) and *on*-times (right). The *off*-times are fitted to a power law, either on a linear scale dominated by short *off*-times (red line) or on a  $\log_{10}$ – $\log_{10}$  scale dominated by long *off*-times (blue line). The corresponding exponents are indicated. The *on*-times probability densities are best fitted by a truncated power law with an exponent,  $\alpha_{\text{on}} = 1.46$ , and a truncation time,  $\tau_c^{\text{on}} = 1.35$  s.

Instruments Cascade 512F or PhotonMAX). The fluorescence intensity of each blinking source was determined in each frame throughout the entire movie (for details see Supporting Information). Following fluorescence imaging, we located NRs relative to the nearest gold markers using TEM (JEOL 2010 or JEOL 2010F) (Figure 1). TEM was always performed after the fluorescence measurements to avoid sample contamination and degradation.

Figure 2 shows one example of an individual NR, oriented approximately parallel to the laser polarization direction (Figure 2b). The fluorescence intensity versus time (also referred to as “intensity trajectory”),  $I(t)$ , recorded over  $2.4 \times 10^4$  s, shows intermittency with relatively short *on*-times ( $< 4$  s) and long *off*-times up to  $\sim 1700$  s (Figure 2c). We

identify the threshold above which the NR is considered “on” using the mean,  $m_{\text{dark}}$ , and standard deviation,  $\sigma_{\text{dark}}$ , of the intensity versus time of a nearby dark region, shown in Figure 2d.

To examine the effect of the choice of threshold on the *on*- and *off*-time probability densities, we analyzed the trajectories using a range of threshold values. All results reported in this paper were determined using a threshold of  $m_{\text{dark}} + 7\sigma_{\text{dark}}$  (dashed blue lines in parts c and d of Figure 2), chosen to lie above the signal from the dark regions. Setting the threshold higher or lower by  $\sigma_{\text{dark}}$  (blue solid lines in Figure 2d) does not change the *on*-/*off*-time probability densities significantly (Table S1 in Supporting Information).

Below we analyze the *on*- and *off*-time probability densities. For *on*-times, we observe a truncated power-law dependence,

$$P(t_{\text{on}}) \propto t_{\text{on}}^{-\alpha_{\text{on}}} e^{-t_{\text{on}}/\tau_{\text{c}}^{\text{on}}}$$

where  $\alpha_{\text{on}} \sim 1.5$  and  $\tau_{\text{c}}^{\text{on}} \sim 1.4$  s (Figure 2e, right).<sup>11,12</sup> We find that  $\tau_{\text{c}}^{\text{on}}$  is the parameter most sensitive to the threshold level; it changes by  $\sim 10\%$  over the threshold range investigated (Figure 2d), while the other parameters change by less than 1% (more details in Table S1 in Supporting Information).

We now focus on the *off*-times, for which the Levy distribution without truncation

$$P(t_{\text{off}}) \propto t_{\text{off}}^{-\alpha_{\text{off}}}$$

has been routinely observed in previous studies. The *off*-time probability density for an individual NR (Figure 2e, left) indeed approximately follows a power law

$$P(t_{\text{off}}) \propto t_{\text{off}}^{-\alpha_{\text{off}}^{\text{lin}}}$$

with  $\alpha_{\text{off}}^{\text{lin}} \sim 1.2$ , obtained by fitting a power law to the data on a linear scale (red line). If a line is fit to  $\log_{10}P(t_{\text{off}})$  versus  $\log_{10}t_{\text{off}}$ , we find a larger power-law exponent,  $\alpha_{\text{off}}^{\text{log}} \sim 1.6$  (blue line). Such a fitting accounts more accurately for the longer *off*-events, while both fitting approaches have been used in the blinking literature.<sup>13</sup>

We find that the Levy process does not hold indefinitely and is also truncated, but on a much longer time scale than the *on*-times. To determine the truncation time, we measured 22 other  $2.4 \times 10^4$  s long intensity trajectories of single NRs. The unprecedented length of our measurements reveals the previously unobserved truncation of the Levy distribution of the *off*-times for single NRs. Figure 3 shows a truncated power-law fit

$$P(t_{\text{off}}) \propto t_{\text{off}}^{-\alpha_{\text{off}}} e^{-t_{\text{off}}/\tau_{\text{c}}^{\text{off}}}$$

to the *off*-time probability density for the aggregated data from all the individual NRs measured. The data and the truncated power-law fit (red) clearly fall below the power-law fit (blue dashed) by roughly a decade in the tail of the distribution. The truncated power-law fits give values of  $\alpha_{\text{off}} = 1.56$  and  $\tau_{\text{c}}^{\text{off}} \sim 1100$  s for the single NR (shown in Figure 2), and  $\alpha_{\text{off}} = 1.78$  and  $\tau_{\text{c}}^{\text{off}} = 2500$  s for the aggregated data. A truncated Levy *off*-time distribution with such a long cutoff is consistent with the results of ensemble measurements on spherical nanocrystals,<sup>14</sup> and truncated Levy *off*-

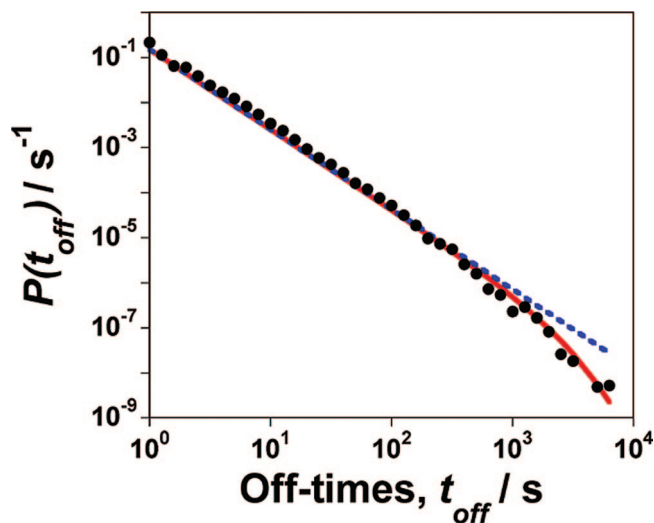


**Figure 3.** *Off*-time probability density of the aggregated data from all 23 individual NRs measured for  $2.4 \times 10^4$  s. The data are best fitted by a truncated power law (red),  $P(t_{\text{on}}) \propto t_{\text{on}}^{-\alpha_{\text{on}}} e^{-t_{\text{on}}/\tau_{\text{c}}^{\text{on}}}$  with  $\alpha_{\text{off}} \sim 1.78$  and  $\tau_{\text{c}}^{\text{off}} \sim 2500$  s. The power-law fit (blue dashed line) is indicated for comparison.

time distributions with much shorter truncation times have recently been observed in nanowires.<sup>1b</sup>

Of all the fluorescent sources examined with TEM,  $\sim 25\%$  correspond to small clusters of two or more NRs, sufficiently close together that the particles cannot be resolved by optical microscopy. Figure 4 shows three examples of the fluorescence intensity versus time,  $I(t)$ , and corresponding TEM images of another individual NR and two small NR clusters: (a) one individual NR oriented at an angle  $\sim 35^\circ$  relative to the laser polarization direction, (b) two NRs aligned parallel to each other, spaced by  $\sim 10$  nm, oriented  $\sim 15^\circ$  relative to the laser polarization direction, and (c) three NRs, spaced by  $\sim 50$ – $100$  nm, oriented at  $0^\circ$ ,  $45^\circ$ , and  $40^\circ$  relative to the polarization direction, respectively. Note that these intensity trajectories are shorter, 1500 s long, and thus show more detail. The examples in Figure 4 illustrate that an individual NR (Figure 4a) and small clusters (Figure 4b,c) can exhibit visually similar intensity trajectories.<sup>15</sup> Furthermore, the observed broad intensity distribution of these trajectories does not necessarily indicate multiple particles but rather demonstrates a continuous distribution of emission states even for a single NR, rather than a single “on” state, as discussed by Zhang et al.<sup>17</sup>

Figure 4d shows the *off*- and *on*-time probability densities,  $P(t_{\text{off}})$  and  $P(t_{\text{on}})$ , and the corresponding fits for clusters of two NRs (cf. Figure 4b) and three NRs (cf. Figure 4c), respectively. The threshold above which the NRs are considered “on” is defined as in the case of single NRs, and the consistency of fitting parameters is verified for a range of threshold values as detailed in the Supporting Information. Similar to individual NRs, we find a power-law dependence of the *off*-times, where  $\alpha_{\text{off},2}^{\text{lin}} \sim \alpha_{\text{off},3}^{\text{lin}} \sim 1.3$ , and a truncated power-law dependence of the *on*-times for the two and three NRs with a truncation time in the range of  $\tau_{\text{c}}^{\text{on}} \sim 1$ – $2$  s. A linear fit to the *off*-time probability densities on a  $\log_{10}$ – $\log_{10}$  scale yields larger values of the power-law exponents,  $\alpha_{\text{off},2}^{\text{log}}$

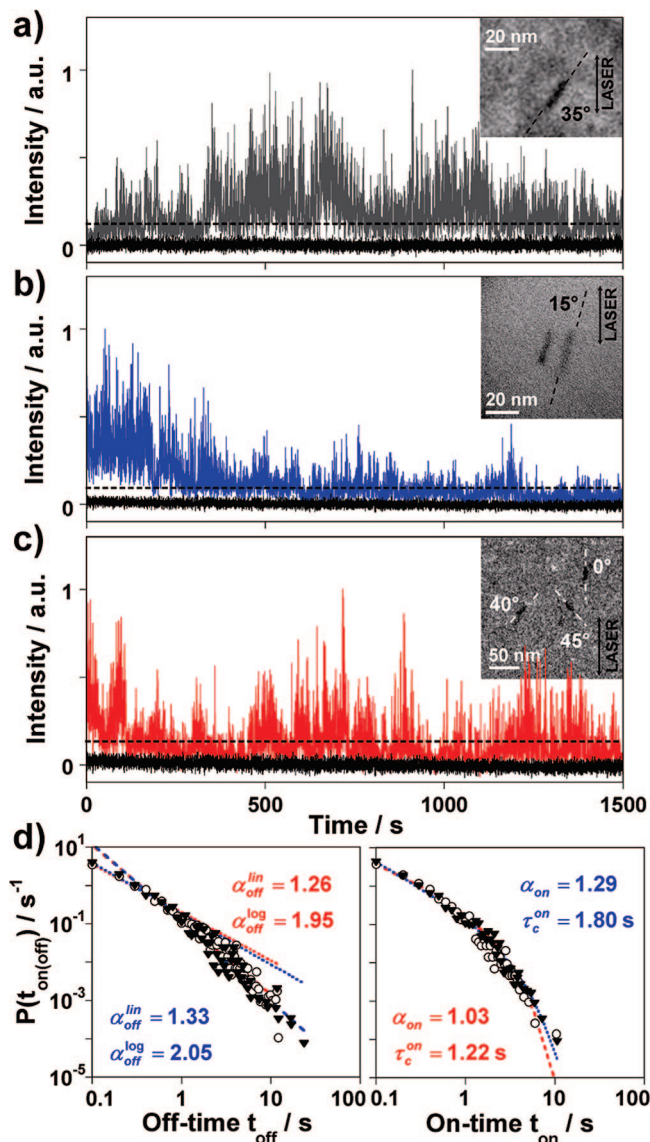


**Figure 4.**  $I(t)$  and corresponding TEM images of (a) an individual NR, (b) two parallel NRs,  $\sim 10$  nm apart, and (c) three randomly oriented NRs, spaced between  $\sim 50$  and  $\sim 100$  nm. The relative orientation with respect to the laser polarization is indicated in each case. Fluorescence intensity vs time,  $I(t)$ , of nearby dark regions are also shown in each case (black curves). (d) *Off*-time and *on*-time probability densities for the two clusters, comprised of two (blue) and three (red) NRs, respectively. The fitting parameters for the truncated power law (*on*-times) and power law (*off*-times) are indicated (see also Table 1).

$\sim \alpha_{off,3}^{log} \sim 2$  for the two and three NRs, respectively. In comparison, the probability density analysis of the individual NR intensity in Figure 4a yields very similar parameters,  $\alpha_{off}^{lin} \sim 1.4$  and  $\alpha_{off}^{log} \sim 2.3$ , and the truncation time for *on*-events,  $\tau_c^{on} \sim 3$  s (Figure S5 in Supporting Information). It can be noted that the downward bending of the *off*-times probability densities is less pronounced than that in Figure 3, since the total measurement interval, 1500 s, is shorter than the truncation time determined above. The exact values of these blinking parameters are listed in Table 1 together with the mean parameter values obtained from the analysis of several clusters containing one, two, or three NRs, respectively. The maximum *off*-time,  $t_{off}^{max}$ , for  $N = 1$  is

**Table 1.** Blinking Parameters of Individual NRs ( $N = 1$ ) and Small NR Clusters Up to  $N = 15$

	$N^a = 1^b$	$N = 2^b$	$N = 3^b$	$N = 5$	$N = 7$	$N = 10$	$N = 15$
$\alpha_{on}$	1.46	1.29	1.03	1.36	1.48	1.29	1.40
	(1.46)	(1.46)	(1.19)				
$\tau_c^{on}/s$	1.35	1.80	1.22	35.9	40.0	26.8	487.7
	(1.40)	(2.38)	(4.00)				
$\alpha_{off}^{lin}$	1.22	1.33	1.26	1.38	1.39	1.35	1.46
	(1.26)	(1.28)	(1.32)				
$\alpha_{off}^{log}$	1.57	2.05	1.95	1.86	2.02	1.91	2.15
	(1.69)	(1.75)	(1.98)				

<sup>a</sup>  $N$  is the number of NRs in one cluster. <sup>b</sup> The indicated values correspond to the clusters shown in Figures 2, 4b and 4c, whereas the italic numbers in parentheses are the averages determined from all observed events with the same  $N$  (i.e., 24 for  $N = 1$ , 4 for  $N = 2$ , and 2 for  $N = 3$ ).

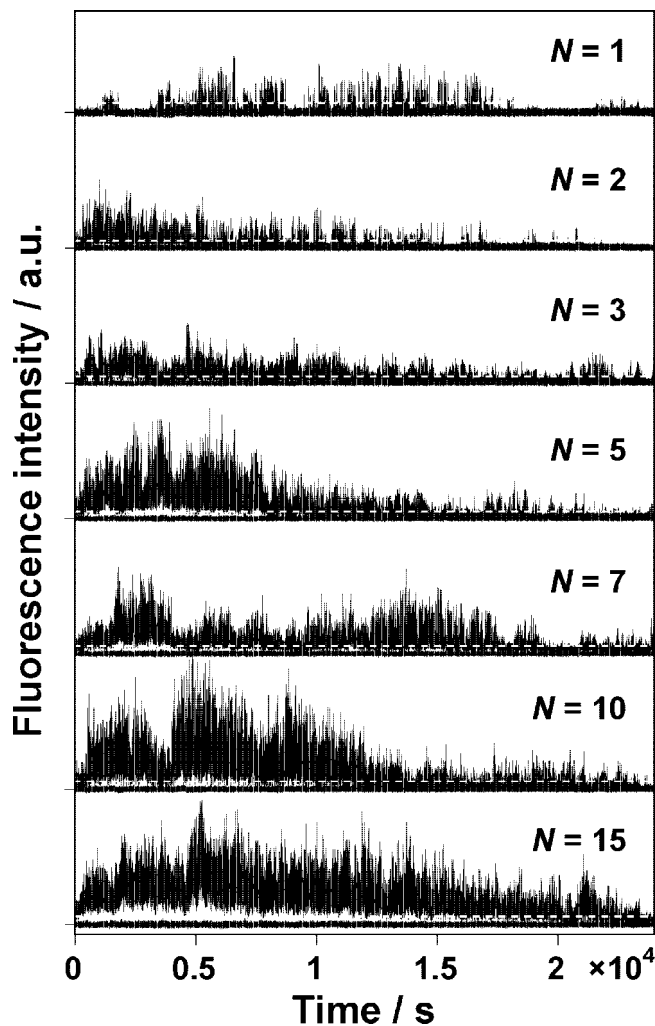


**Figure 5.** Fluorescence intensities vs time,  $I(t)$ , in order of increasing particle number,  $N = 1$  to 15, with their corresponding background signals (gray curves) and threshold levels (dashed lines), recorded over  $\sim 2.4 \times 10^4$  s.

smaller than those of  $N = 2$  and  $N = 3$  (20 s vs 38 and 25 s), while the maximum *on*-time,  $t_{on}^{max}$ , for  $N = 1$  is smaller than that of  $N = 2$  (20 s vs 25 s) but larger than that of  $N = 3$  (20 s vs 16 s). On the basis of these parameters, the trajectories cannot be a priori attributed to a particular  $N$ .

Among the  $\sim 2.4 \times 10^4$  s long fluorescence measurements, using TEM we have identified 23 individual blinking NRs and 8 additional blinking sources that correspond to NR

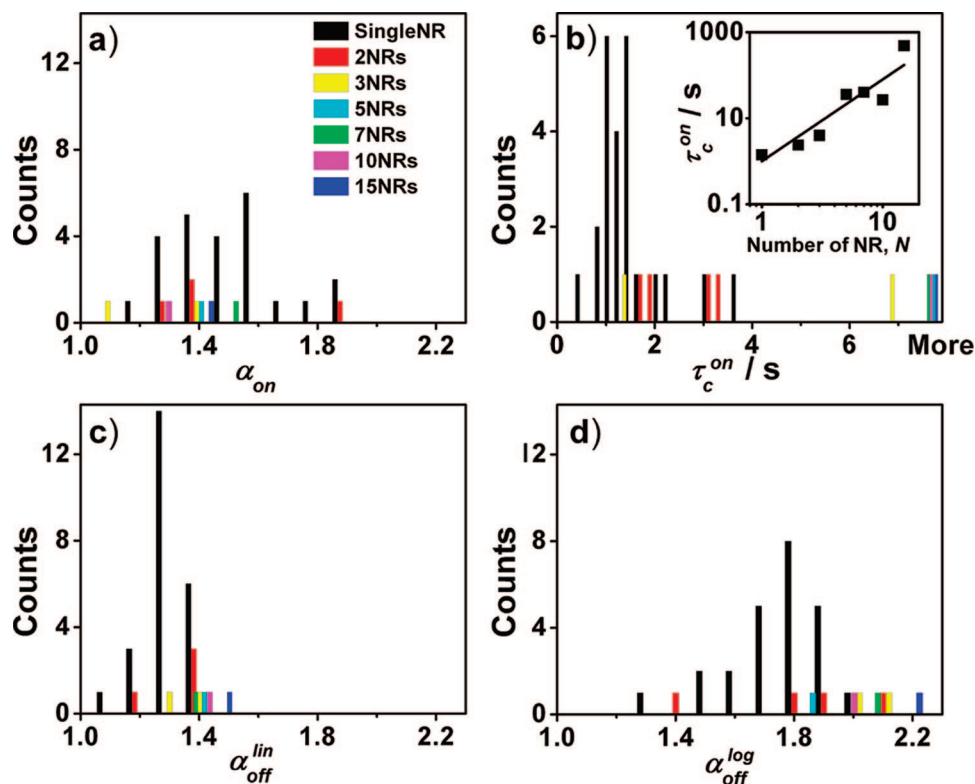


**Figure 6.** Histograms of the blinking parameters (a)  $\alpha_{on}$ , (b)  $\tau_c^{on}$ , (c)  $\alpha_{off}^{lin}$ , and (d)  $\alpha_{off}^{log}$  for 24 individual NRs and 10 additional blinking sources that correspond to NR clusters consisting of up to 15 NRs, including also the spots measured only for 1500 s (shown in Figure 4). The values of  $\alpha_{off}$  (i.e.,  $\alpha_{off}^{lin}$  and  $\alpha_{off}^{log}$ ) for  $N \geq 2$  fall above the mean values of the corresponding distributions of single NRs, while the values of  $\alpha_{on}$  for  $N > 2$  fall within those obtained for individual NR. Inset of (b):  $\tau_c^{on}$  vs  $N$  on a  $\log_{10}$ – $\log_{10}$  scale.  $\tau_c^{on}$  increases to  $\sim 30$  s for  $N = 5$ – $10$  and up to  $\sim 500$  s for  $N = 15$  (solid line shows the best fit to the data,  $\tau_c^{on} \sim N^{1.9}$ ).

clusters consisting of up to  $N = 15$  NRs. The sizes of these clusters range from  $\sim 40$  nm ( $N = 2$ ) to  $\sim 300$  nm ( $N = 15$ ) in diameter. Figure 5 displays seven fluorescence intensities versus time,  $I(t)$ , in order of increasing number of particles,  $N = 1, 2, 3, 5, 7, 10,$  and  $15$ , with their corresponding background signals and threshold levels. While the intensity trajectories for small  $N$  are visually similar, larger  $N$  clusters exhibit visibly larger intensities for larger  $N$ ; in addition, the maximum *off*-time in Figure 5 decreases (from  $t_{off}^{max} \sim 2200$  s ( $N = 1$ ) to  $\sim 70$  s ( $N = 15$ )), while the maximum *on*-time increases (from  $t_{on}^{max} \sim 7$  s ( $N = 1$ ) up to  $\sim 3000$  s ( $N = 15$ )). In addition, for clusters with larger  $N$ , the trajectory is visibly elevated above the baseline.

Figure 6 shows the histograms of blinking parameters  $\alpha_{on}$ ,  $\tau_c^{on}$ , and  $\alpha_{off}$  (i.e.,  $\alpha_{off}^{lin}$  and  $\alpha_{off}^{log}$ ) determined for all the fluorescence data, both individual NRs and clusters. From the histograms for the individual NRs (black bars in Figure 6), we obtained the means and standard deviations of the blinking parameters to be  $\alpha_{off}^{lin} = 1.26 \pm 0.06$ ,  $\alpha_{off}^{log} = 1.7 \pm 0.2$ ,  $\alpha_{on} = 1.5 \pm 0.2$ , and  $\tau_c^{on} = 1.4 \pm 0.6$  s.<sup>18</sup>

We have also sampled the *on*- and *off*-time probability distributions of single NRs throughout a  $\sim 6$  h long measurement by dividing it into three 2 h long segments and sampling the corresponding probability distributions. This analysis showed that probability distributions of single NRs do not change significantly over time and that no systematic trends of the blinking parameters are evident. In turn, this also implies that the average fluorescence intensity decrease that

is apparent for some cluster trajectories in Figure 5 could be due to statistical aging of ensembles.<sup>14</sup>

Correlated TEM imaging also allows for the direct measurement of NR angles relative to the laser polarization by aligning the polarization direction with the gold markers on the substrate. Analyses of the single-NR blinking parameters  $\alpha_{on}$ ,  $\tau_c^{on}$ ,  $\alpha_{off}^{lin}$ , and  $\alpha_{off}^{log}$  as a function of the NR angle relative to the laser polarization,  $\theta$  (Figure S6 in the Supporting Information), suggest no apparent correlation between these quantities. However, any potential angle dependence of the blinking parameters that may exist might not be observable because of the variation of blinking parameters across the single NRs measured (black bars in Figure 6). We also measured a series of 600 s long fluorescence movies of  $\sim 80$  single NRs in which successive movies alternated between two orthogonal linear polarizations of the laser excitation. These measurements did not reveal any clear dependence of the blinking parameters on polarization direction. Moreover, these measurements suggest that any potential dependence of blinking parameters on polarization direction may be small and that its observation may require long measurements for each polarization direction to obtain more accurate values of the blinking parameters. In addition, our preliminary measurements comparing NR blinking with circular and linear polarization showed similar distributions of truncation times. All of these results suggest that the effect of polarization is simply to affect the effective excitation intensity and are consistent with the weak

intensity dependence of the blinking parameters we reported previously.<sup>3</sup> Further measurements are underway to conclusively address this issue.

The broad distribution of single-NR blinking parameters means that the *on*- and *off*-exponents for clusters fall within the range of the values observed for single NRs. In addition, the observed values of  $\tau_c^{\text{on}}$  for  $N = 2$  or  $3$  lie within the observed range of single NR blinking parameters, indicating that probability density analysis *cannot* be used as a reliable way to distinguish between single NRs and small clusters; only direct particle counting allows us to unambiguously distinguish single particles from small clusters ( $N = 2, 3$ ). Similarly, we find that the integrated intensity<sup>19</sup> from  $N = 2$  clusters is indistinguishable from the range of integrated intensities observed from single NRs. Other methods of analysis such as the autocorrelation function also did not reveal differences between single NRs and clusters (Figure S10 in Supporting Information). In contrast, ref 7 finds that autocorrelation function analysis can be used to distinguish between individual quantum dots and quantum dot clusters. They attribute the difference to interparticle interactions possibly arising from the close packing of quantum dots and a different sample preparation method. However, that work did not address differences that may exist in the blinking parameters, thus not allowing a comparison with our finding of the particle number dependence of the truncation times of the *on*-time probability density.

We do, however, observe increasing  $\tau_c^{\text{on}}$  with increasing particle number for  $N > 3$ . The inset of Figure 6b shows the mean  $\tau_c^{\text{on}}$  for a given  $N$  plotted versus  $N$  on a  $\log_{10}$ – $\log_{10}$  scale. While the mean  $\tau_c^{\text{on}}$  is  $\sim 1.4$  s for individual NRs, it increases to  $\sim 30$  s for  $N = 5$ – $10$  and up to  $\tau_c^{\text{on}} \sim 500$  s for  $N = 15$ ; an empirical fit to the data indicates that  $\tau_c^{\text{on}}$  grows faster than  $N$  (the line shown corresponds to  $\tau_c^{\text{on}} \sim N^{1.9}$ ). Additionally, the values of  $\alpha_{\text{off}}$  (Figure 6c,d) for  $N > 2$  all fall above the mean values of the corresponding distributions obtained from single NRs. These trends, which are observed regardless of the choice of threshold (see Supporting Information), are consistent with larger  $N$  increasing the probability of long *on*-events (i.e., larger  $\tau_c^{\text{on}}$ ) and the maximum *on*-time, and decreasing the probability of long *off*-events (i.e., larger  $\alpha_{\text{off}}^{\text{lin}}$  and  $\alpha_{\text{off}}^{\text{log}}$ ) and the maximum *off*-time.

The distance between NRs within the clusters studied was highly variable, varying from  $\sim 1$ – $10$  nm to  $\sim 50$ – $100$  nm. Based only on these distances, it is impossible to completely exclude interparticle interactions. While direct charge tunneling between NRs is very unlikely, due to the relatively large interparticle separations, it is difficult to a priori exclude a role for longer-range dipole–dipole interactions and energy transfer between NRs,<sup>20</sup> given that blinking occurs on very long time scales and thus relatively weak interactions could still have an effect. Studies on clusters with well-controlled NR orientations and spacing, as well as clusters of NRs capped with various ligands, are currently in progress to further examine the effect of nanoparticle interactions on blinking dynamics. While the increase in *on*-times in a cluster can be attributed to combining uncorrelated *on*-events from

different nanocrystals, detailed analysis of the *on*-time distribution may shed light on the possibility of some sort of correlations in blinking statistics due to interactions between nanocrystals within a cluster. Such a study is beyond the scope of this work.

In summary, we compared blinking statistics of individual nanoparticles and that of nanoparticle clusters with the number of NRs in the cluster determined by TEM imaging. We find that *off*- and *on*-time probability density analysis and autocorrelation function analysis do not unambiguously distinguish between single and multiple particle clusters of two and three particles. Direct determination of the particle number,  $N$ , is therefore important to distinguish single particles from those of small clusters. However, clusters of five or more NRs can be distinguished from single NRs by their significantly larger  $\tau_c^{\text{on}}$ . Finally, facilitated by very long fluorescence measurements, we have estimated the truncation time of the Levy distribution of *off*-times for single NRs to be of order 2000 s.

**Acknowledgment.** This work was supported by Alfred P. Sloan Fellowship, NSF (NSF Career Award DMR-0449533, NSF CCF05-08346, NSF NSEC DMR-0425780, MRSEC DMR05-20020), and ONR (YIP N000140410489 and N000140510393). L.W. acknowledges funding from the NSF-IGERT program (Grant DGE-0221664). D.N. was supported by NSF Grants DMR-0749220 and DMR-0754613. We thank Dr. Ken Healy for helpful discussions.

**Supporting Information Available:** Details of NR synthesis and characterization, statistical analyses of intensity trajectories, a comparative study of fitting methods and threshold levels, and their influence on the statistical parameters, additional examples of intensity trajectories of individual NRs and small clusters, dependence of blinking parameters on NR angle relative to the laser polarization direction, autocorrelation function analysis. This material is available free of charge via the Internet at <http://pubs.acs.org>.

## References

- (1) For a recent reviews see: (a) Cichos, F.; von Borczyskowski, C.; Orrit, M. *Curr. Opin. Colloid Interface Sci.* **2007**, *12*, 272–284, and references therein. (b) Frantsuzov, P.; Kuno, M.; Janko, B.; Marcus, R. A. *Nat. Phys.* **2008**, *4*, 519–522, and references therein.
- (2) See for example: Nirmal, M.; Dabbousi, B. O.; Bawendi, M. G.; Macklin, J. J.; Trautman, J. K.; Harris, T. D.; Brus, L. E. *Nature* **1996**, *383*, 802–804.
- (3) Wang, S.; Querner, C.; Emmons, T.; Drndic, M.; Crouch, C. H. *J. Phys. Chem. B* **2006**, *110*, 23221–23227.
- (4) (a) Protasenko, V. V.; Hull, K. L.; Kuno, M. *Adv. Mater.* **2005**, *17*, 2942–2949. (b) Glennon, J. J.; Tang, R.; Buhro, W. E.; Loomis, R. A. *Nano Lett.* **2007**, *7*, 3290–3295.
- (5) See for example: (a) Messin, G.; Hermier, J. P.; Giacobino, E.; Desbiolles, P.; Dahan, M. *Opt. Lett.* **2001**, *26*, 1891–1893. (b) Brokmann, X.; Hermier, J. P.; Messin, G.; Desbiolles, P.; Bouchaud, J. P.; Dahan, M. *Phys. Rev. Lett.* **2003**, *90*, 120601.
- (6) Issac, A.; von Borczyskowski, C.; Cichos, F. *Phys. Rev. B* **2005**, *71*, 161302.
- (7) Yu, M.; Van Orden, A. *Phys. Rev. Lett.* **2006**, *97*, 237402.
- (8) Koberling, F.; Mews, A.; Philipp, G.; Kolb, U.; Potapova, I.; Burghard, M.; Basche, T. *Appl. Phys. Lett.* **2002**, *81*, 1116–1118.
- (9) The core NRs were synthesized using a multiple injection method and subsequently capped with an intermediate ZnSe shell and an outer ZnS shell. The experimental details are provided in the Supporting Information. The fluorescence quantum yield, estimated with respect

- to Rhodamine 6G, increased from 0.3% (core) to a maximum of 10% (core/shell).
- (10) Fischbein, M. D.; Drndic, M. *Appl. Phys. Lett.* **2006**, *88*, 063116.
- (11)  $\alpha_{\text{on}}$  is determined by fitting a power-law through the first four points ( $t_{\text{on}} < 1$  s) according to the procedure described in ref 12, which gives good fits and consistent fitting parameters for different emitters.
- (12) Tang, J. *J. Phys. Chem. A* **2007**, *111*, 9336–9339.
- (13) For a linear fit see for example: Kuno, M.; Fromm, D. P.; Hamann, H. F.; Gallagher, A.; Nesbitt, D. J. *J. Chem. Phys.* **2000**, *112*, 3117–3120, For a power-law fit to the data on a linear scale see for example ref 3 and the discussion therein.
- (14) Chung, I.; Bawendi, M. G. *Phys. Rev. B* **2004**, *70*, 165304.
- (15) However, it has to be noted that the intensity trajectories should be compared with caution since the NRs are not oriented at the same angles. As NRs couple to the laser field predominantly along their long axis, the emission intensity,  $I$ , depends on the angle,  $\theta$ , between the NR long axis and the laser polarization:  $I \sim \cos^2 \theta$ .<sup>16</sup> As an example, rotating the laser polarization by 90° in the case of the two NRs, shown in Figure 4b, decreased their maximum emission intensity to ~10% of the initial integrated intensity as  $\theta$  increased from ~15° to ~75°, which is in good agreement with the expected angle dependence. Details for this and a few other examples are given in the Supporting Information.
- (16) (a) Chen, X.; Nazzal, A.; Goorskey, D.; Xiao, M.; Peng, A.; Peng, X. *Phys. Rev. B* **2001**, *64*, 245304. (b) Hu, J. T.; Li, L. S.; Yang, W. D.; Manna, L.; Wang, L. W.; Alivisatos, A. P. *Science* **2001**, *92*, 2060–2063.
- (17) Zhang, K.; Chang, H.; Fu, A.; Alivisatos, A. P.; Yang, H. *Nano Lett.* **2006**, *6*, 843–847.
- (18) The obtained values of  $\alpha_{\text{off}}$  and  $\alpha_{\text{p}}$  are close to those previously reported for NR blinking on mica (cf. ref 3). However, the characteristic time  $\tau_c^{\text{on}}$  associated with the exponential decay is shorter for Si<sub>3</sub>N<sub>4</sub> ( $\tau_c^{\text{on}} = 1.3$  s) compared to mica ( $\tau_c^{\text{on}} = 4.0$  s).
- (19) The integrated intensity was calculated as

$$I_{\text{int}} = \left( \sum_{n=1}^N I_n \right) / N$$

where  $I_n$  is the intensity count after the background subtraction, for the  $n^{\text{th}}$  time interval of 0.1 s.

- (20) (a) Xu, L.; Xu, J.; Ma, Z.; Li, W.; Huang, X.; Chen, K. *Appl. Phys. Lett.* **2006**, *89*, 0331212. (b) Kimura, J.; Uematsu, T.; Maenosono, S.; Yamaguchi, Y. *J. Phys. Chem. B* **2004**, *108*, 13258–13264. (c) Crooker, S. A.; Hollingsworth, J. A.; Tretiak, S.; Klimov, V. I. *Phys. Rev. Lett.* **2002**, *89*, 186802. (d) Shabaev, A.; Efros, A. L. *Nano Lett.* **2004**, *4*, 1821–1825. (e) Pons, T.; Medintz, I. L.; Sykora, M.; Mattoussi, H. *Phys. Rev. B* **2006**, *73*, 245302. (f) Shubeita, G. T.; Sekatskii, S. K.; Dietler, G.; Potapova, I.; Mews, A.; Basche, T. *J. Microsc.* **2003**, *210*, 274–278. (g) Muller, F.; Gotzinger, S.; Gaponik, N.; Weller, H.; Mlynek, J.; Benson, O. *J. Phys. Chem. B* **2004**, *108*, 14527–14534.

NL802696F